Parameter Estimation in Finite Element Simulations of Rayleigh Waves

A. Zerwer[1]; G. Cascante[2]; and J. Hutchinson[3]

Abstract: Spectral analysis of surface waves measurements are used to develop subsurface soil profiles or as a tool to delineate abandoned crown pillar structures. Finite element modeling of Rayleigh waves has practical application in simulating SASW measurements. Developing a reliable and accurate finite element model to simulate Rayleigh waves requires the proper mesh dimensions and attenuation parameters. This research proposes a new simplified methodology for quantifying mesh dispersion effects. In addition, methods of verifying damping ratios for numerical simulations are presented. The evaluation of an array of nodal displacements in the frequency–wave-number domain effectively illustrates mesh dispersion effects and the presence of parasitic modes of vibration. Calculations of damping ratio show that mass and stiffness damping parameters are valid within a specified frequency bandwidth. The new techniques are tested for a half-space model; however, they can be used for the analysis of layered media. In addition, equations are given for the calculation of linear Rayleigh damping. These equations satisfy the conditions of an average damping with minimum variance within the frequency bandwidth of interest.

DOI: 10.1061/(ASCE)1090-0241(2002)128:3(250)

CE Database keywords: Rayleigh waves; Finite element method; Damping; Wave propagation.

Introduction

The spectral analysis of surface waves (SASW) technique is based on the analysis of vibrations created by Rayleigh waves that propagate along the surface of a medium. Velocity dispersion of Rayleigh waves is used to provide near-surface soil profiles (Rix and Stokoe 1989). The SASW methodology is also applied to the detection of abandoned near-surface crown and pillar structures (Cascante et al. 1999; Phillips et al. 2000). Closed-form solutions for the propagation of Rayleigh waves through complex subsurface media do not exist. Therefore, numerical solutions, such as finite elements, are the only alternative to measuring the effectiveness of the SASW method for anomaly detection (Gucunski and Woods 1992).

The Newmark-β method is a useful and versatile finite element tool for modeling Rayleigh wave propagation. A finite element model applied to this application requires mesh parameters and constants representing material behavior. Quite often, the mesh design and selection of appropriate model parameters to obtain accurate results is time-consuming. One method of developing a finite element simulation is to select the model parameters and quantify the accuracy of the results. The user may then decide to amend the model or continue using it.

The accuracy and stability of finite element models are primarily affected by the spatial-temporal discretizations within the mesh. In the spatial domain, finite mesh dimensions cause the removal of short-wavelength (high-frequency) energy. Low-pass filtering by the mesh can produce spurious oscillations, known as Gibb's phenomenon, as well as velocity dispersion. To minimize the effects of mesh filtering, the maximum mesh size is calibrated to the wavelength of the slowest propagating wave. In the temporal domain, improper discretization can cause instability and frequency aliasing for propagating waveforms (Valliappan and Murti 1984). Wang et al. (1992) illustrated the interdependence of spatial-temporal discretizations on velocity dispersion. They found that propagation velocity decreases for smaller mesh sizes and that it increases for smaller time increments.

Analytical approaches exist to assess the stability and accuracy of a finite element model (Marfurt 1984). In general, these techniques examine the effect of one modal component within the finite element model. Such methods are estimations when complex mesh geometries are proposed.

Another important factor influencing the numerical accuracy of finite element simulations is the treatment of damping. Two types of attenuation are encountered in finite element models: numerical and material attenuation. The Newmark-β integration parameters cause numerical attenuation, whereas Rayleigh damping parameters provide linear material attenuation. Numerical and material attenuation must be balanced to obtain an accurate model. Furthermore, the Rayleigh damping parameters must be carefully chosen because this formulation only approximates field or laboratory measurements (Woodward and Griffiths 1996).

The purpose of this study is to introduce an innovative method to quantitatively evaluate mesh limitations and damping effects of a finite element model applied to simulating transient wave propagation. Mesh filtering effects are studied using a linear array of vertical nodal displacements that are two dimensionally Fourier-

[1]Research Associate, Dept. of Civil Engineering, Univ. of Waterloo, ON, Canada.

[2]Assistant Professor, Dept. of Civil Engineering, Univ. of Waterloo, ON, Canada.

[3]Assistant Professor, Dept. of Geological Sciences and Geological Engineering, Queen's Univ., ON, Canada; formerly, Dept. of Earth Sciences, Univ. of Waterloo, ON, Canada.

Note. Discussion open until August 1, 2002. Separate discussions must be submitted for individual papers. To extend the closing date by one month, a written request must be filed with the ASCE Managing Editor. The manuscript for this paper was submitted for review and possible publication on March 16, 2001; approved on August 7, 2001. This paper is part of the ***Journal of Geotechnical and Geoenvironmental Engineering***, Vol. 128, No. 3, March 1, 2002. ©ASCE, ISSN 1090-0241/2002/3-250–261/$8.00+$.50 per page.

transformed. Damping effects are examined by calculating the attenuation generated by finite element models using power spectrum ratios. The reliability of these techniques is assessed using the analytical solution of Lamb's problem for the vertical time history of a Rayleigh wave. Subsequently, the methodology is tested on a finite element package (*ABAQUS*) by modeling the propagation of Rayleigh waves in an infinite half-space.

The results show that frequency–wave-number representations can clearly quantify velocity dispersion and determine the efficiency of nonreflecting (silent) boundaries. In addition, the spectral ratio technique is shown to be effective in measuring absolute and relative damping ratios generated by the finite element model. Finally, equations are presented for the calculation of Rayleigh damping parameters such that a given average damping ratio and a minimum variance are specified in the frequency range of interest.

First, fundamental concepts concerning spatial-temporal discretization and the relationship between numerical and material damping are examined. Lamb's problem is described next. This analytical solution is used to verify the presented signal-processing techniques. Then, finite element model definitions and results are elaborated in detail, followed by a discussion of the proposed methodology for quantifying mesh and damping effects.

Discretization and Damping

The effects of spatial-temporal discretization and damping can be analyzed for a single element. The interdependence between wave velocity, maximum mesh dimension, and time increment are discussed in the following sections. Next, the relationship between numerical damping and Rayleigh damping is examined. These equations will provide an estimate of element dimensions for subsequent finite element simulations.

Spatial-Temporal Discretization

In wave propagation problems, element dimensions are chosen with respect to the highest frequency ($f_{\max}$) for the lowest velocity wave (V_R). Element dimensions that are too large will filter high frequencies, whereas very small element dimensions can introduce numerical instability as well as require considerable computational resources. An approximate element dimension (g) is calculated using

$$g \leqslant \chi \lambda_{\min} \tag{1}$$

where

$$\lambda_{\min} = \frac{V_R}{f_{\max}}$$

where $\lambda_{\min}$=minimum wavelength. The constant χ must be less than 0.5 because of the Nyquist limit, and further it depends on whether the mass matrices are consistent ($\chi = 0.25$) or lumped ($\chi = 0.2$). This formulation assumes that elements have square dimensions (Valliappan and Murti 1984; Saenger et al. 2000).

The time increment must be carefully chosen to maintain numerical stability and accuracy. Numerical instability may cause the solution to diverge if the time increment is too large. Conversely, a very short time increment can cause spurious oscillations (Gibb's phenomenon). The calculation of the time increment depends on the element dimension computed with the following expression:

$$\frac{1}{10}\frac{g}{V_P} \leqslant \tau \leqslant \frac{g}{V_P} \tag{2}$$

where τ = characteristic time; g = mesh dimension [Eq. (1)]; and V_P = compression wave velocity (Valliappan and Murti 1984). Although the characteristic time incorporates the spatial Nyquist limit, the characteristic time must also consider the temporal Nyquist limit ($f_{\max} < 1/2\Delta t$).

Damping

Attenuation (or damping) has various quantitative expressions depending on application. Relevant mathematical relations for damping are shown in Table 1. Attenuation can be divided into measures for acoustic waves and measures found in numerical simulations. Acoustic waves are subject to geometric damping where the source energy spreads through a larger volume. Geometric damping is a function of distance from the source and wave type. Acoustic waves also attenuate because of damping related to the material properties of the medium. Material damping can be measured in the time and frequency domains.

Two types of attenuation can be distinguished in finite element modeling: numerical and material attenuation. Numerical attenuation is caused by the Newmark-β parameters controlling the time integration scheme. The default values of the Newmark-β parameters in *ABAQUS* add a small amount of numerical damping to ensure solution convergence. Numerical damping is also caused by the mesh, which removes wavelengths shorter than the Nyquist limit. The material damping is user-defined and controls the energy dissipation per cycle. This study examines the linear Rayleigh damping model, which will be described in detail.

In dynamic finite element analysis, the governing equation of motion is expressed as

$$[M]\{\ddot{u}\} + [C]\{\dot{u}\} + [K]\{u\} = \{F\} \tag{3}$$

where $\ddot{u}$, $\dot{u}$, and u are the acceleration, velocity, and displacement vectors, respectively. The mass matrix is given by M, the viscous damping matrix is C, and the stiffness matrix is K. Although energy principles are used to evaluate the mass (M) and stiffness (K) matrices, the damping matrix (C) is not easily incorporated into the finite element solution unless simplifying assumptions are made. Finite element schemes overcome this problem by decoupling the equations of motion. Caughey (1960) showed that the damping matrix could be expressed as a linear combination of the mass and stiffness matrices. This type of damping is referred to as Rayleigh damping and is given by

$$[C] = [M]\sum_{k=0}^{p} \eta_{k+1}\left(\frac{[K]}{[M]}\right)^k \tag{4}$$

given that η is a constant. By setting $p = 1$, the standard Rayleigh damping equation is obtained (Liu and Gorman 1995)

$$[C] = \eta_1[M] + \eta_2[K] \tag{5}$$

where η_1 and η_2 are constants for the mass and stiffness, respectively. The relationship between damping ratio and Rayleigh damping is given by

$$D = \frac{\eta_1}{2\omega} + \frac{\eta_2 \omega}{2} \tag{6}$$

where D = damping ratio. The relation shown in Eq. (6) refers to a single degree of freedom or a single mode of vibration. The relationship between damping ratio (Rayleigh damping) and the relevant frequency range is shown in Fig. 1.

To incorporate linear damping into a finite element model, the approach is to curve fit η_1 and η_2 values to model the damping of

J. Geotech. Geoenviron. Eng., 2002, 128(3): 250-261

Table 1. Damping Relationships for Wave Propagation and Numerical Models

Wave propagation model	Damping type	Relationship	Variables
	Geometric	$1/d^2$ body waves at the surface $1/\sqrt{d}$ Rayleigh waves	d = distance from the source
Theoretical wave propagation	Material (time domain)	$2D=1/Q=\alpha_t T/\pi=\alpha_x\lambda/\pi$	D = damping ratio Q = quality factor α_t = coefficient of attenuation (time) α_x = coefficient of attenuation (space)
	Material (frequency domain)	$D=\frac{[\ln(A_1/A_2)-\ln(G_1/G_2)]V}{2\pi fx}$	$\ln(A_1/A_2)$ = spectral ratio $\ln(G_1/G_2)$ = geometric damping V = velocity f = frequency x = distance
	Numerical (time)	α,β	α, β = Newmark-β parameters
Numerical simulations	Numerical (spatial)	$g\leqslant\chi(V_R/f_{\max})$	g = element dimension χ = const V_R = Rayleigh wave velocity $f_{\max}$ = maximum frequency
	Material (Rayleigh damping)	$D=(\eta_1/2\omega)+(\eta_2\omega/2)$	η_1 = mass damping parameter η_2 = stiffness damping parameter ω = circular frequency

the predominant vibration modes (Léger and Dussault 1992; Woodward and Griffiths 1996). Therefore, η_1 and η_2 are given by

$$\eta_1=\frac{2D(\omega)\omega_1\omega_n}{\omega_1+\omega_n},\quad \eta_2=\frac{2D(\omega)}{\omega_1+\omega_n} \tag{7}$$

where ω_1 and ω_n are generally taken as the first natural frequency (ω_1) and the highest natural frequency (ω_n) of the vibration modes with high contribution to the response. The value for ω_n is chosen to represent 90–95% of the modal mass, which is calculated from the eigenvalues of the system.

In certain applications, damping is constant over a certain frequency range; however, constant attenuation cannot be achieved using the Rayleigh damping parameters. Over the bounded frequency range suggested by Eq. (7), the average damping ratio is less than the specified value. To obtain a more reliable estimate, the average damping ratio within the bounded frequency range should be used to define the Rayleigh damping parameters. Furthermore, the specified Rayleigh damping should have a minimum variance. It can be shown that the average damping between ω_1 and ω_n is given by

$$\overline{D}=\frac{\left[\frac{\eta_1}{2}\ln\left(\frac{\omega_1}{\omega_n}\right)+\frac{\eta_2}{4}(\omega_n^2-\omega_1^2)\right]}{\omega_n-\omega_1} \tag{8}$$

where $\overline{D}$ = average damping. The variance is given by

$$\sigma=\frac{(\omega_n-\omega_1)\left[\frac{\eta_1^2}{4}\left(\frac{1}{\omega_1}-\frac{1}{\omega_n}\right)+\frac{\eta_2^2}{12}(\omega_n^3-\omega_1^3)+\frac{\eta_1\eta_2}{2}(\omega_n-\omega_1)\right]-\overline{D}^2}{(\omega_n-\omega_1)^2} \tag{9}$$

By choosing an average damping ratio, a relation for either the mass or stiffness damping can be calculated with Eq. (8). Then Eq. (9) is used to find the other Rayleigh parameter that provides the minimum variance.

Analysis Methodology

This section addresses two main issues in finite element simulations of wave propagation: the optimum element size and the evaluation of the actual damping in the model. The finite element mesh and damping parameters are tested with two separate signal-processing techniques. A frequency–wave-number analysis applied to vertical nodal displacements will highlight dispersion effects caused by the mesh. Damping generated by the finite element model is examined with power spectral ratios. Both methods are tested using the analytical solution to Lamb's problem for the vertical displacement of a Rayleigh wave.

Lamb's Problem

Lamb (1904) calculated the far-field vertical and horizontal displacement histories generated by a point source on an infinite

J. Geotech. Geoenviron. Eng., 2002, 128(3): 250-261

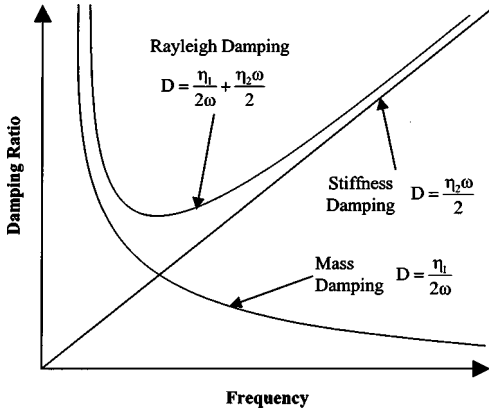

Fig. 1. Relationship between Rayleigh damping parameters and damping ratio

half-space. Separate analytical solutions for compression, shear, and Rayleigh waves are superposed to generate a realistic time history. Only the solution to Rayleigh wave displacements is used in this study.

The analytical solution to Lamb's problem for Rayleigh wave displacements is given by Båth and Berkhout (1984). Loading is simulated using a point source acting on the surface of an infinite half-space given by

$$F(t) = \frac{F_b t}{\pi(t^2 + \psi^2)} \tag{10}$$

where F_b alters the force magnitude, ψ controls the width of the pulse (i.e., frequency content), and t represents time. Rayleigh wave vertical displacements are calculated using

$$w(t,d) = \frac{RF_b}{4\pi G\psi^2 V_R}\sqrt{\frac{2\psi V_R}{d}}\cos\left(\frac{\pi}{4} - \frac{3}{2}v\right)\cos^{3/2}(v) \tag{11}$$

given

$$v = \tan^{-1}\left(\frac{t - \frac{d}{V_R}}{\psi}\right) \tag{12}$$

where R = a constant dependent on compression, shear, and Rayleigh wave velocities; V_R = Rayleigh wave velocity; G = shear modulus; and d = distance from the source. The loading function used in this study and the typical vertical displacements of a Rayleigh wave are shown in Fig. 2.

Array Signal Processing

Numerical dispersion of different wave types can be computed using array measurements. Vertical nodal displacements calculated at equidistant surface nodes define a receiver array. Displacement time histories are assembled into a matrix where each column represents amplitude in time and each row defines amplitude in space. Applying a two-dimensional Fourier transform to the matrix converts the data into the frequency–wave-number domain (*f-k* plots). A hamming window is applied in both the temporal and spatial directions to reduce frequency leakage. Magnitude values of each element in the transformed matrix are used to generate a contour plot. Peaks in the contour plot correspond to the various wave types, and their trends are used to measure the dispersive properties of the finite element mesh. Peaks are represented by solid dots in the contour plots (Zerwer et al. 2000).

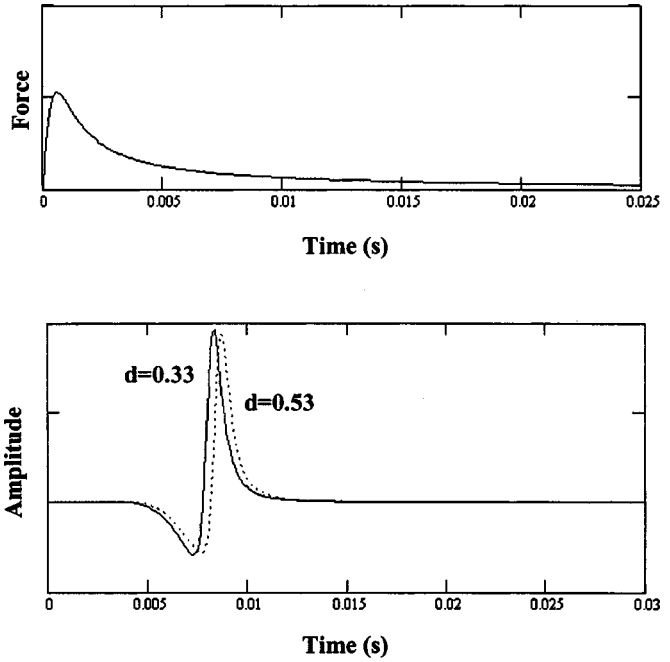

Fig. 2. Loading function and vertical displacement of Rayleigh wave from solution of Lamb's problem

Array dispersion measurements are illustrated with the solution to Lamb's problem for Rayleigh waves. A series of 49 equidistant time histories are used as input. Distance between measurements is 10 mm, with a sampling interval of 1×10^{-4} s (f_{max}=5 kHz). The Rayleigh wave shown in Fig. 3 is nondispersive (i.e., all peaks can be joined by a straight line), as predicted by the solution to Lamb's problem.

An important feature of frequency–wave-number plots is the ability to retrieve wave directionality. Because the two-dimensional Fourier transform is rotationally invariant, waves traveling through the array from right to left or vice versa can be distinguished. The frequency–wave-number plots are divided into two segments. To the right of the wave number $k=0$ are waves traveling left-right (direct wave) through the array, whereas waves

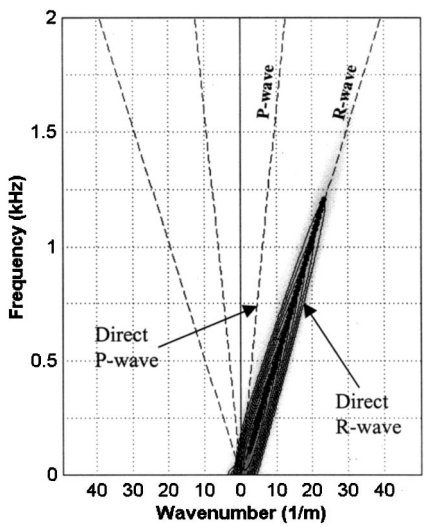

Fig. 3. Frequency–wave-number plot of Rayleigh wave with time histories generated by solution to Lamb's problem

J. Geotech. Geoenviron. Eng., 2002, 128(3): 250-261

traveling right-left along the array are to the left of $k=0$ (reflected wave). Fig. 3 shows the direct wave with no reflections, because there are no peaks to the left of $k=0$.

Damping Calculations

Spectral ratios are the most common technique for calculating damping in wave propagation problems. Spectral amplitudes of a plane wave can be represented by

$$A(f)=\mathrm{Ge}(x)e^{-\alpha(f)x} \tag{13}$$

where A=amplitude; f=frequency; Ge is a term that includes geometrical spreading and reflections; x=distance; and $\alpha(f)$ =attenuation coefficient. If measurements are made at two separate locations, the ratio of Fourier amplitudes can be expressed as

$$\frac{A_1}{A_2}=\frac{\mathrm{Ge}_1}{\mathrm{Ge}_2}e^{[\alpha_1(f)x_2-\alpha_1(f)x_1]} \tag{14}$$

The subindex denotes the receiver number. Eq. (14) can be rewritten as

$$\ln\left(\frac{A_1}{A_2}\right)-\ln\left(\frac{\mathrm{Ge}_1}{\mathrm{Ge}_2}\right)=\alpha_2(f)x_2-\alpha_1(f)x_1 \tag{15}$$

The first term on the left-hand side of Eq. (15) represents the power spectrum ratio and the second term accounts for geometric damping. Material attenuation is considered on the right-hand side of Eq. (15) (Ward and Toksöz 1971; Toksöz et al. 1979).

Eq. (15) can be used to define a measure of absolute damping or relative damping. Absolute damping refers to measurements made at different locations on the same finite element model (i.e., $\alpha_1=\alpha_2$). The geometric attenuation is zero for two-dimensional finite element models. In terms of damping ratio (D), absolute damping is defined as

$$D=\frac{V_R\ln\left(\frac{A_1}{A_2}\right)}{2\pi f\Delta x} \tag{16}$$

where V_R=Rayleigh wave velocity and Δx=distance between the two measurements. Relative damping compares the attenuation at the same location (i.e., $x_1=x_2$) for two different finite element models. In this case, both models are identical except for the Rayleigh damping parameters. Relative damping (ΔD) is defined as the difference in attenuation between two different materials

$$\Delta D=\frac{V_R\ln\left(\frac{A_1}{A_2}\right)}{2\pi fx} \tag{17}$$

where x is the distance from the source. Absolute damping is calculated for subsequent finite element simulations to compare damping generated by a finite element model to attenuation measured in a field or laboratory setting. Relative damping is compared with absolute damping to examine the effectiveness of the Rayleigh damping model.

Absolute damping calculations are validated using Lamb's solution for Rayleigh waves. For receiver spacings of $x_1=0.42$ m and $x_2=0.44$ m, the amplitude ratio of the Rayleigh wave is

$$\sqrt{\frac{x_2}{x_1}}=1.02 \tag{18}$$

Fig. 4 shows that the amplitude spectral ratio calculated using Eq. (14) is equal to the geometric damping ratio accounted for by Lamb's solution.

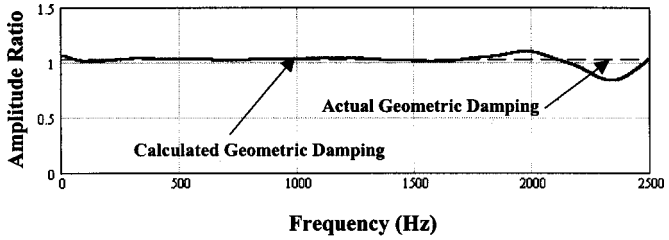

Fig. 4. Measurement of geometric damping of Rayleigh wave using absolute damping calculation

Finite Element Simulations

The array and damping measurement techniques are applied to a series of finite element models. Rayleigh wave dispersion is examined using two mesh designs. One mesh is composed of rectangular elements each having identical dimensions. The second mesh is graded in the vertical direction, with smaller elements near the surface where the Rayleigh wave is propagating. Both mesh designs have the same number of elements and are surrounded on three sides by nonreflecting elements to represent an infinite half-space. The Newmark-β and Rayleigh damping parameters are altered similarly for uniform and graded mesh designs to examine the effect of numerical attenuation on the damping measurements. The uniform and graded mesh designs are shown in Fig. 5.

The following paragraphs provide details of the elastic material parameters, the mesh design, and the time increment. Values of numerical damping and Rayleigh damping for the different finite element simulations are listed. Finally, results from the various simulations are discussed.

Model Parameters

Input parameters for the finite element model are chosen to simulate a series of laboratory experiments completed on a box filled with dry sand. The body and Rayleigh wave velocities in the dry sand are $V_P=170$ m/s (compression), $V_S=60$ m/s (shear), and $V_R=56$ m/s (Rayleigh). The bulk density is computed as $\rho=1{,}656$ kg/m^3, assuming a void ratio of $e=0.6$ and a specific gravity of $G=2.65$. Young's modulus and the shear modulus are calculated using the wave velocities and the computed Poisson ratio of $\nu=0.43$. The relatively high Poisson ratio is a result of the low confinement ($\sigma_0\approx 0$) at the surface of the sand box. Young's modulus is calculated as $E=16.8$ MPa and the shear modulus is $G=5.88$ GPa.

The uniform mesh is designed by first calculating the maximum mesh dimension. As shown in Eq. (1), the maximum dimension depends on the Rayleigh wave velocity, the highest propagating frequency, and the constant χ. Laboratory measurements show the frequency bandwidth to be between 0.2 and 1 kHz ($\lambda_{\min}=56$ mm). The value of χ is 0.25 for the consistent mass approach used by *ABAQUS*, which gives a maximum dimension of 14 mm. Therefore, elements are 10 mm in the horizontal direction and 14 mm in the vertical direction, giving 3,196 elements within the solution domain. There are the same number of elements in the graded mesh, where the only difference is that element dimensions are between 5 and 55 mm in the vertical direc-

J. Geotech. Geoenviron. Eng., 2002, 128(3): 250-261

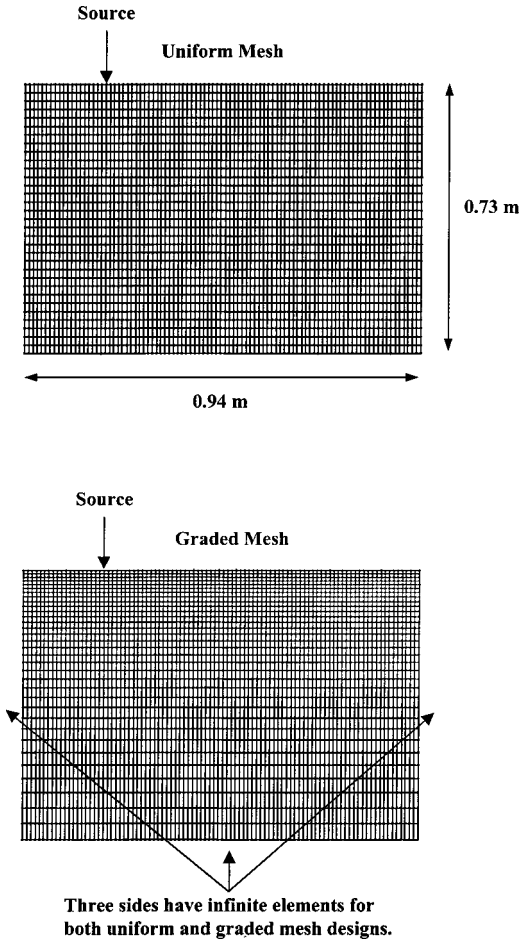

Fig. 5. Uniform and graded mesh designs

tion. Smaller elements are near the surface, whereas larger elements are located at the bottom of the mesh. Elements used have bilinear interpolation functions.

The time increment is computed using Eq. (2). With a maximum element dimension of 14 mm, the largest time increment is 8.2×10^{-5} s and the smallest time increment is 8.2×10^{-6} s. The time increment used in these simulations is 1×10^{-5} s (Nyquist frequency = 50 kHz).

The loading function used to generate the Rayleigh wave is calculated with Eq. (10) ($F_b=2\times10^{-6}$, $\psi=6$). Comparison of time-domain traces in Fig. 6 shows a good agreement between the solution to Lamb's problem and the finite element results (model 11), as well as some numerical dispersion of the finite element model. A typical series of time-domain traces for different nodal locations are shown in Fig. 7. The same loading function is used

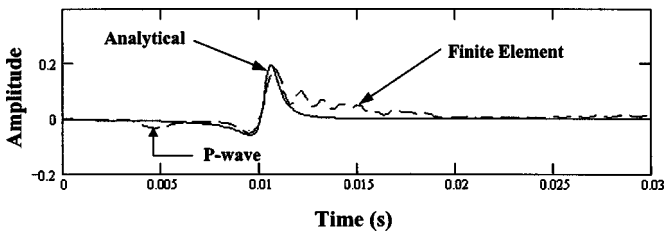

Fig. 6. Comparison between analytical solution for Rayleigh wave and finite element result

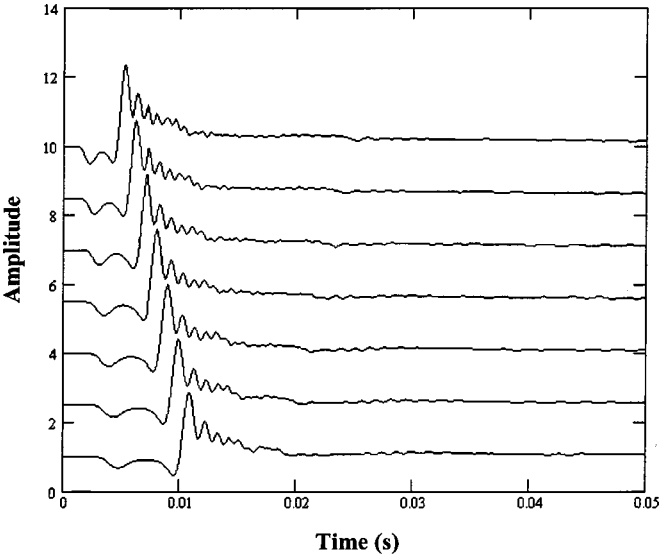

Fig. 7. Time history measurements from series of nodal locations (200, 250, 300, 350, 400, 450, and 500 mm from source)

for all subsequent simulations. The oscillations in the finite element response are effects of the spatial and time discretization. The relative amplitude of the *P* wave is small because of the source type (i.e., vertical impulse). A horizontal impulse in an infinite half-space would generate a stronger *P* wave.

Damping is examined through various finite element simulations where numerical and Rayleigh damping are added. As shown in Table 2, initial finite element simulations have no nu-

Table 2. Listing of Finite Element Simulations

Model number	Mesh grading	Rayleigh damping η_1	Rayleigh damping η_2	Avg. damping (%)[a]
1	Uniform	0	0[b]	0
2		0	0	0
3		0	5×10^{-6}	0.94
4		100	0	1.6
5		13.7	1.49×10^{-6}	0.5
6		27.5	2.97×10^{-6}	1
7		82.4	8.92×10^{-6}	3
8	Graded	0	0[b]	0
9		0	0	0
10		0	1×10^{-6}	0.19
11		0	5×10^{-6}	0.94
12		0	1×10^{-5}	1.88
13		0	5×10^{-5}	9.42
14		5	0	0.08
15		50	0	0.8
16		100	0	1.6
17		150	0	2.4
18		200	0	3.2
19		13.7	1.49×10^{-6}	0.5
20		27.5	2.97×10^{-6}	1
21		82.4	8.92×10^{-6}	3

[a]Average damping calculated between 0.2 and 1 kHz [Eq. (8)].

[b]No numerical damping (Newmark-β parameters, $\alpha=0.5$, $\beta=0.25$). Default values of ($\alpha=0.55$, $\beta=0.28$) are used for all other models.

J. Geotech. Geoenviron. Eng., 2002, 128(3): 250-261

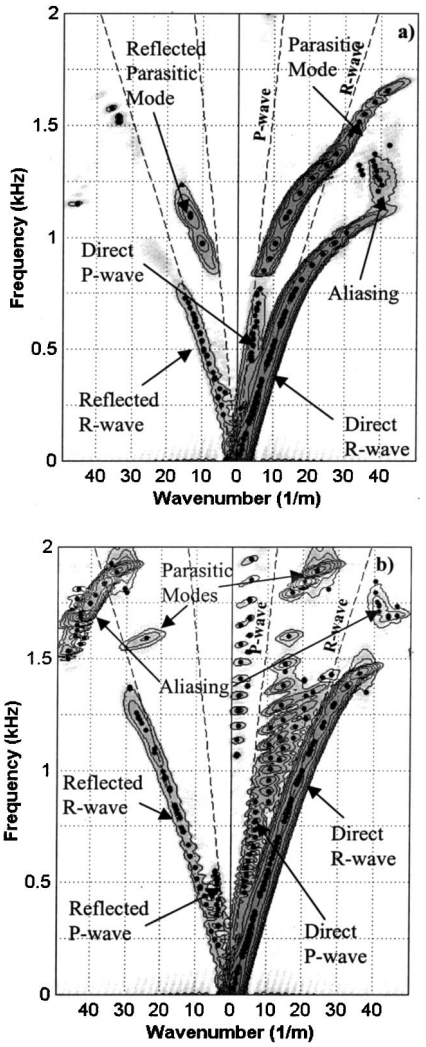

Fig. 8. Frequency–wave-number plot of Rayleigh wave: (a) uniform mesh with no damping; (b) graded mesh with no damping

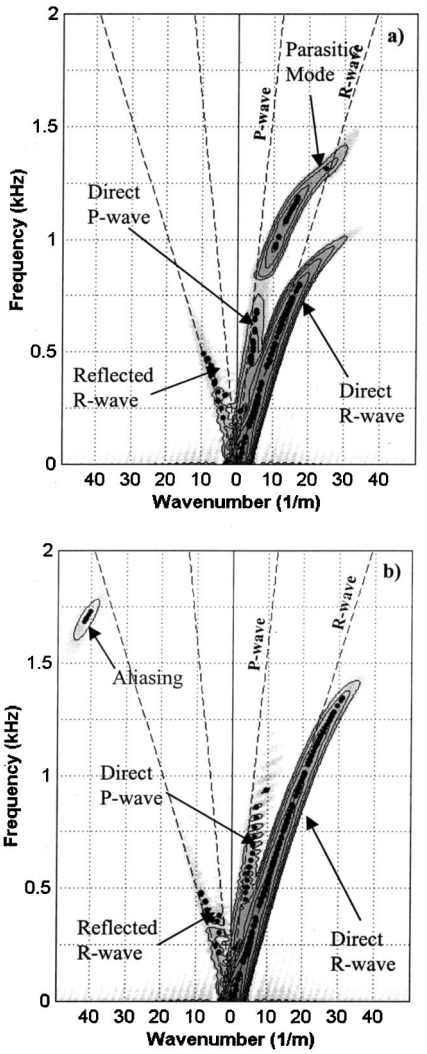

Fig. 9. Effect of stiffness damping on Rayleigh wave propagation ($\eta_2 = 5 \times 10^{-6}$): (a) uniform mesh; (b) graded mesh

merical damping and material damping (models 1 and 8). The next model uses the default numerical damping with no material damping (models 2 and 9). Subsequent models include numerical damping with mass and stiffness damping altered separately (models 3–7 and 10–21). Absolute damping calculations are made between nodes located 330 and 530 mm from the source. The measurement locations are chosen to maximize the distance from the source to minimize signal contamination caused by any near-field effects. In addition, a large receiver spacing (d) is required to allow accurate measurement of longer wavelengths. Conflicting criteria exist for the selection of the maximum reliable wavelength with standards ranging from $\frac{1}{2}d$ to $3d$ (Al-Hunaidi 1993). The receiver spacing (d) is the criterion used for this work. Therefore, with a wavelength of 200 mm, the minimum reliable measurement frequency is 280 Hz. The models with no numerical or material damping specified are used as a control model to calculate the relative damping.

Finally, several simulations examine the ability of the finite element model to simulate constant damping for low-strain wave propagation (Cascante and Santamarina 1997). Rayleigh damping parameters for these simulations are calculated using Eqs. (8) and (9). Mean damping ratios, with minimum variance, are $\frac{1}{2}$, 1, and 3% between 0.2 and 1 kHz.

Simulation Results

The frequency–wave-number plots clearly illustrate the onset of numerical dispersion. As shown in Fig. 8(a) (model 1), the dispersion of the Rayleigh wave begins at 0.6 kHz for a uniform mesh without numerical and material damping. Also shown in this plot is a direct compression wave up to a frequency of 0.75 kHz and a weak reflected Rayleigh wave. Spatial aliasing of the Rayleigh is visible above 1.1 kHz. Another important feature is the presence of a strong extraneous numerical (parasitic) mode, above the compression wave, in both the direct and reflected directions. A parasitic mode is an extraneous solution generated by the finite element formulation and is related to the interpolation functions. This mode is parasitic because energy in this part of the frequency–wave-number space should not exist (Marfurt 1984). The only propagating modes that exist in a half-space are nondispersive body and Rayleigh waves (Lamb 1904).

When a graded mesh without damping is used, the dispersion of the direct Rayleigh wave becomes significant at 1 kHz as shown in Fig. 8(b) (model 8). The direct and reflected compression and Rayleigh waves are also observed. Spatial aliasing of the direct and reflected Rayleigh waves occurs at 1.5 kHz. Several parasitic modes are observed in this model.

J. Geotech. Geoenviron. Eng., 2002, 128(3): 250-261

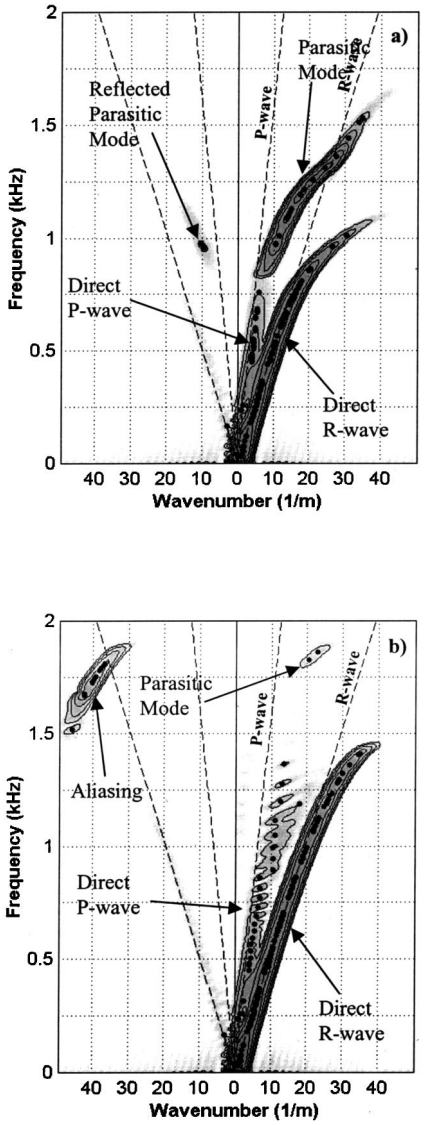

Fig. 10. Effect of mass damping on Rayleigh wave propagation ($\eta_1 = 100$): (a) uniform mesh; (b) graded mesh

The effect of stiffness damping on the uniform mesh is shown in Fig. 9(a) (model 3). Stiffness damping reduced the energy of the direct and reflected parasitic mode as well as the reflected Rayleigh wave. Results for the graded mesh are shown in Fig. 9(b) (model 11). The stiffness damping removed the parasitic mode; however, the reflected Rayleigh wave energy remained.

The effect of mass damping is less pronounced for high frequencies ($f > 1$ kHz). The frequency–wave-number plots for the uniform and graded mesh design are shown in Fig. 10 (models 4 and 16). In both cases, the reflected energy is almost completely removed ($f < 1$ kHz). The uniform mesh still has a strong parasitic component.

Absolute damping measurements are calculated using Eq. (16). Damping ratios calculated using the finite element results of the uniform mesh (models 3 and 4) are compared in Fig. 11 with the solution obtained from Eq. (6). Damping ratios calculated from the finite element model are slightly lower, between 0.28 and 0.6 kHz, than predicted values. Measured damping ratios for stiffness damping are much larger than predicted damping for low frequencies ($f < 200$ Hz). Similar results are obtained for constant damping ratios between 0.2 and 1 kHz [Eqs. (8) and (9)] as

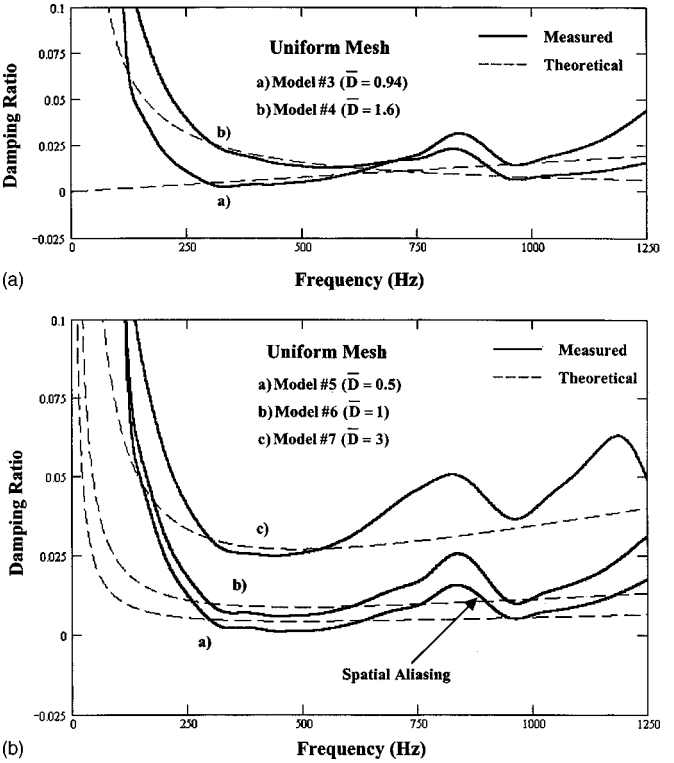

Fig. 11. Absolute damping calculations for (a) mass and stiffness damping on uniform mesh and (b) constant damping on uniform mesh

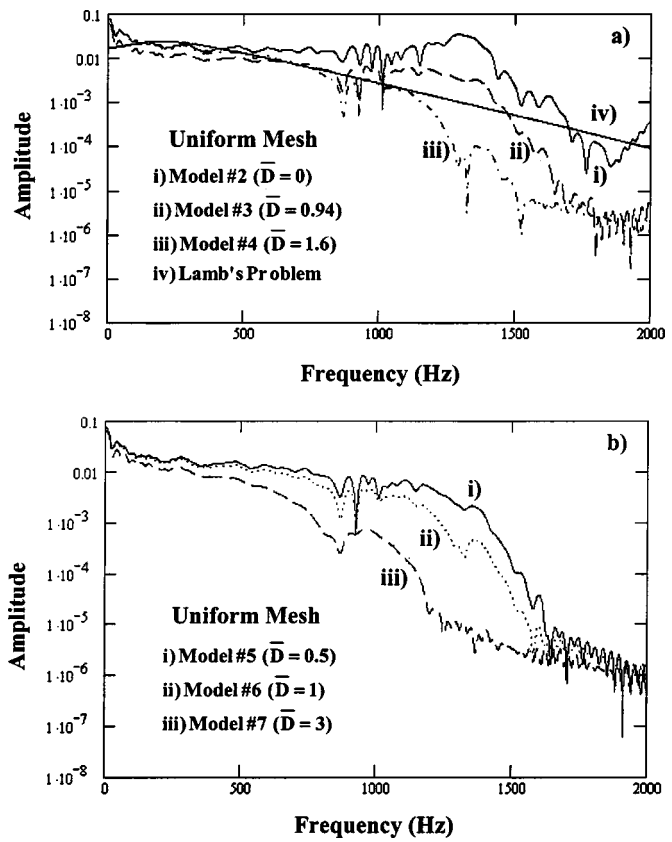

Fig. 12. Power spectrum densities for (a) mass and stiffness damping on uniform mesh and (b) constant damping on uniform mesh

J. Geotech. Geoenviron. Eng., 2002, 128(3): 250-261

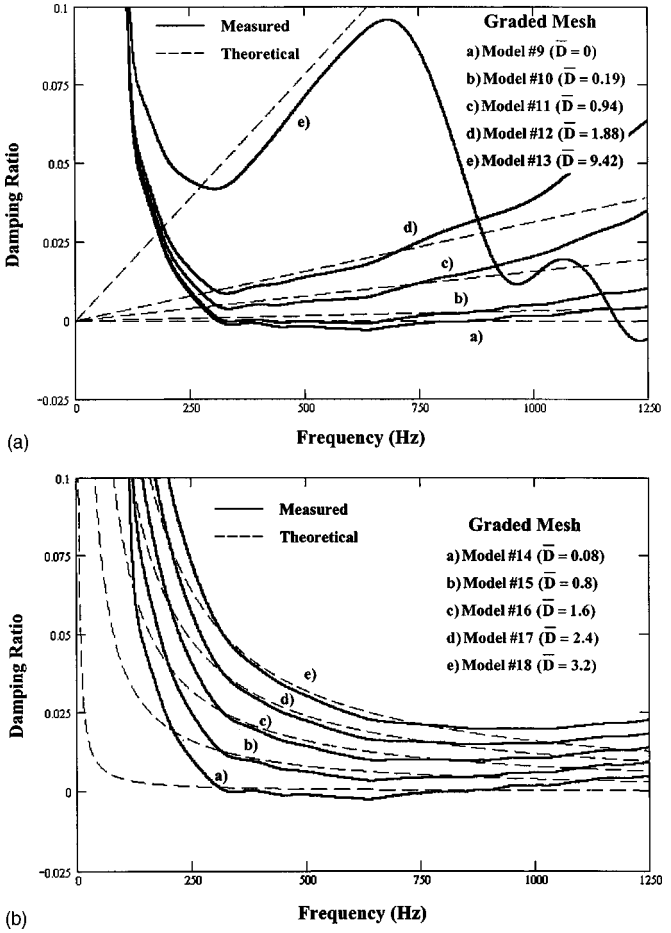

Fig. 13. Absolute damping calculations for (a) stiffness damping on a graded mesh and (b) mass damping on graded mesh

shown in Fig. 11(b). As a comparison, power spectrum measurements for the uniform mesh simulations are shown in Figs. 12(a and b).

Mass and stiffness damping calculations from the finite element model with the graded mesh are shown in Figs. 13(a and b). In all of the cases, the damping ratio calculated between 0.28 and 0.75 kHz from the finite element model is slightly less than the damping ratio computed using Eq. (6). The damping ratio calculated between 0.75 and 1 kHz from the finite element model is higher than the Rayleigh damping model for $\eta_2 < 1 \times 10^{-5}$. As shown in Fig. 14, similar results are obtained when constant damping ratios are used. Power spectrum calculations for all graded mesh simulations are shown in Figs. 15 and 16. Changes in mass and stiffness damping are directly observed in the spectral amplitudes. As expected, stiffness damping has a stronger effect on high frequencies than mass damping.

Relative damping calculations for uniform and graded mesh designs are computed for stiffness damping, mass damping, and constant damping ratio. Typical results for the graded mesh are shown in Fig. 17 and compared to the case of no material damping (model 2). The agreement between damping ratios calculated from the finite element results and the Rayleigh damping [Eq. (6)] is better than the agreement for absolute damping. The relative damping ratio obtained from the finite element model increases above 600 Hz for the uniform mesh and 750 Hz for the graded mesh.

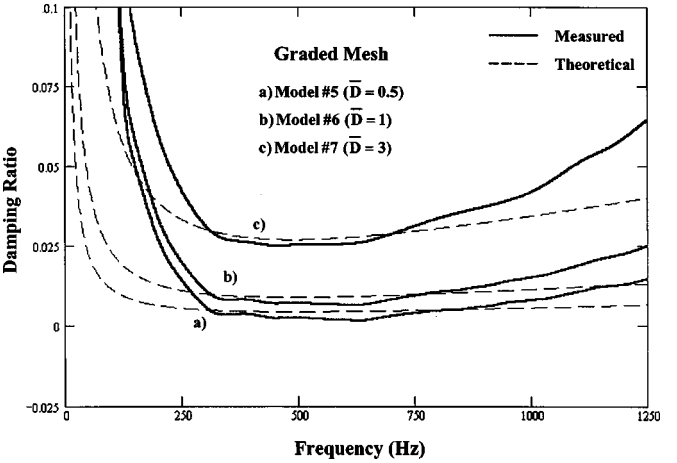

Fig. 14. Absolute damping calculations for constant damping on graded mesh

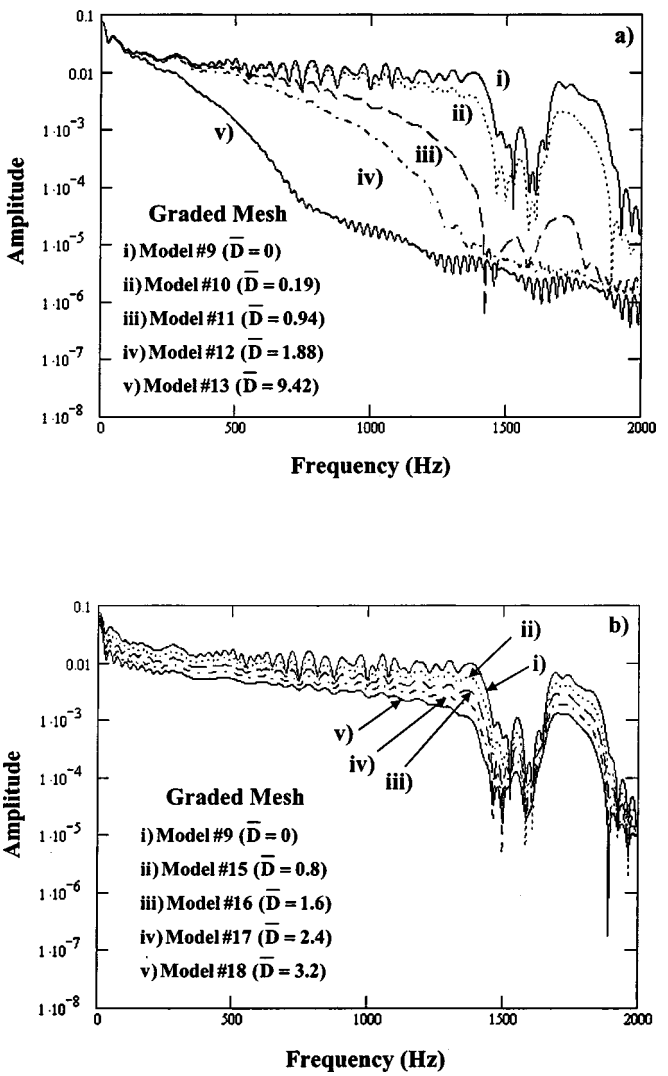

Fig. 15. Power spectrum densities for (a) stiffness damping on graded mesh and (b) mass damping on graded mesh

J. Geotech. Geoenviron. Eng., 2002, 128(3): 250-261

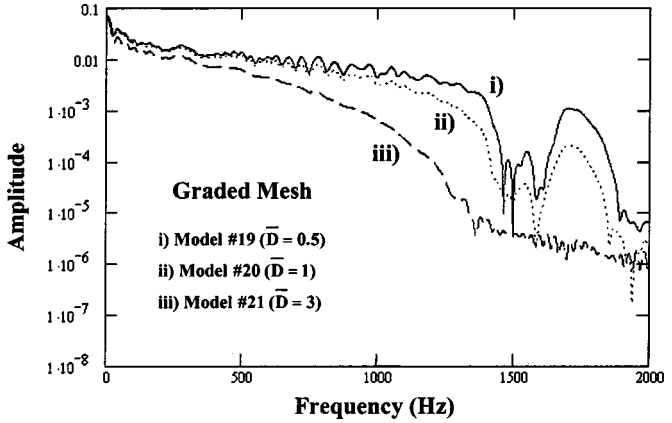

Fig. 16. Power spectrum densities for constant damping on graded mesh

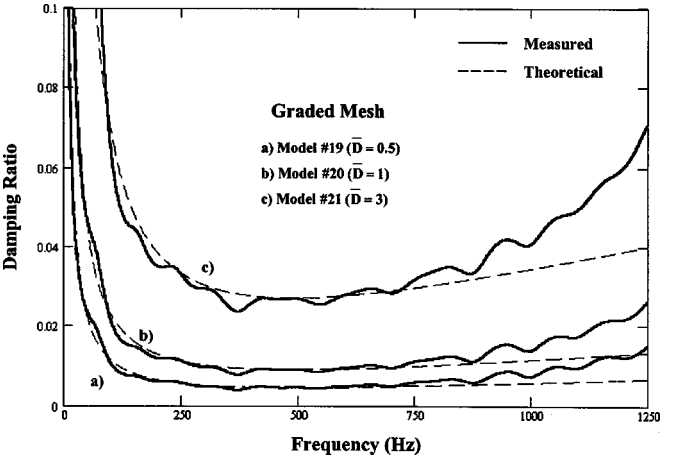

Fig. 17. Relative damping calculations for constant damping on graded mesh. Comparisons are made with the case of no material damping (model 2).

Discussion

The *f-k* plots clearly show the differences between the response of two different mesh designs. The graded mesh provided a more accurate representation of the Rayleigh wave than the uniform mesh for a wider frequency bandwidth. Rayleigh wave dispersion in the uniform mesh occurs at 750 Hz, whereas in the graded mesh dispersion begins at 1 kHz. Grading the mesh in the vertical direction increases the accuracy of the Rayleigh wave. The reason for this is that most of the Rayleigh wave energy is located within one wavelength of the surface.

Plotting the data in the *f-k* domain allows the easy identification of numerical (parasitic) modes. Parasitic modes are generated by the finite element formulation and have no realistic basis. For these simulations, only nondispersive body and Rayleigh waves should be observed in an infinite half-space (Lamb 1904). As shown in Figs. 8–10, this is clearly not the case. These figures illustrate that parasitic modes contain significant energy and may influence simulation results. The presented results show that the effect of numerical modes can be reduced by altering the mesh dimensions or employing stiffness damping. Parasitic modes have a stronger influence in the uniform mesh than in the graded mesh. A parasitic mode begins at 750 Hz in the uniform mesh, whereas a parasitic mode appears at 1.5 kHz in the graded mesh, because the graded mesh is better suited for higher frequencies, as mentioned above.

The uniform mesh results [Fig. 8(a)] show that Rayleigh wave dispersion becomes noticeable at 750 Hz. With a velocity of 56 m/s and a grid dimension of 14 mm, the value of χ would be 0.1875 [Eq. (1)]. This constant is more restrictive than the rule-of-thumb value of 0.25.

The *f-k* plots can also be used to evaluate the effectiveness of the nonreflecting boundary elements. Rayleigh and compression wave reflections are observed for simulations without numerical and material damping. These reflections are present for large values of stiffness damping, but almost disappear when mass damping is applied. The reason for this is that mass damping strongly attenuates lower frequencies (Fig. 10).

Selecting the appropriate mass and stiffness damping parameters is necessary in order to obtain accurate results. Time-domain traces from simulations without numerical or material damping contain high-frequency numerical noise. This effect is observed in the comparison of Lamb's problem with the finite element solution. Furthermore, the power spectrum calculations show that high Rayleigh damping can limit the frequency bandwidth by completely removing high-frequency energy, as shown in Figs. 12(a) and 15(a). The sharp reduction of the damping ratio at 750 Hz [Fig. 13(a), trace *e*] reflects the energy loss caused by a large value of stiffness damping.

Measured absolute damping for the uniform and graded mesh designs is about 0.3% lower than predicted in certain frequency bandwidths. Reduced damping may be caused by insufficient elements. More elements may be required to accurately simulate energy dissipation.

High damping ratios are calculated outside the linear frequency bandwidths. Damping ratios at low frequencies are not representative due to the fact that the damping ratios calculated at low frequencies are sensitive to small changes in spectral amplitude because as $f \rightarrow 0$, $D \rightarrow \infty$ [Eq. (16)]. Furthermore, long-wavelength Rayleigh waves have not fully developed at these distances. Conversely, at high frequencies, damping ratios are higher because of mesh filtering effects. Relative damping calculations confirm these conclusions. A sudden increase of the damping ratio occurs only at very low frequencies, whereas the damping ratio increases at high frequencies, similar to the absolute damping measurements (Fig. 17).

The power spectra shown in Figs. 12, 15, and 16 illustrate the change in signal energy for various Rayleigh damping parameters. Power spectral density decreases as the material damping increases. In addition, the frequency bandwidth containing coherent energy decreases for high damping ratios. The energy dissipation observed in the *f-k* plots and the power spectra are similar.

Theoretical and numerical dispersion curves match within a certain frequency–wave-number bandwidth. Outside these limits, the finite element simulation is no longer accurate. Similarly, Rayleigh wave damping calculations, which are also affected by mesh or time increment dispersion, are not reliable. These results are important for the simulation of SASW tests, because the results from the SASW method directly depend on the simulated dispersion curves.

Observations from half-space simulations can be extended to Rayleigh waves propagating through layered media. Although Rayleigh waves are dispersive in layered media, element size and time increment will also affect finite element simulations as in the half-space case. Element dimensions must be properly chosen to represent Rayleigh wave propagation up to the desired frequency and the presence of parasitic modes must be identified. The pro-

J. Geotech. Geoenviron. Eng., 2002, 128(3): 250-261

posed methodology for the evaluation of damping can be used to assess the average damping for layered media.

Conclusions

The reliability of a finite element model can be determined by recognizing and quantifying its limitations. The main factor affecting the accuracy of wave propagation simulations is the spatial-temporal discretization of a finite element model. In addition, the handling of damping by the finite element model also affects the accuracy. This study proposes a new methodology for determining the frequencies at which numerical dispersion occurs. In addition, a method of measuring absolute and relative damping from finite element results is examined. These techniques are tested on a finite element model simulating a half-space using a uniform and graded mesh, and by varying the damping parameters; however, these techniques can be used for an analysis of layered media.

The frequency–wave-number plots clearly show when numerical dispersion occurs. Frequency–wave-number plots also have the ability to detect the presence of parasitic modes. These plots show that stiffness damping combined with an appropriate mesh design can reduce or eliminate the effect of spatial aliasing, unwanted reflections, and parasitic modes. Mass damping tends to remove reflection energy at low frequencies, leaving the direct propagation modes intact.

Absolute damping measurements show that damping simulated by the finite element model is slightly lower than the damping values input into the finite element model. The absolute damping ratios show a rapid increase at frequencies where the numerical dispersion begins, as indicated in the frequency–wave-number plots. This effect is also observed in the relative damping measurements. The relative damping ratios are in agreement with the Rayleigh damping model up to the frequency at which numerical dispersion begins. Above this frequency, damping ratios rapidly increase. Damping ratios measured at low frequencies are not representative of the true damping ratios. Low-frequency values in the damping calculation cause disproportionately large increases in damping ratio.

This work also proposes new equations for calculating Rayleigh damping parameters for finite element simulations where constant damping is required. Equations for average damping and variance are used to obtain Newmark-β parameters that minimize variance while maintaining an average damping ratio within a specified frequency bandwidth.

Acknowledgments

This research is part of a study on nondestructive testing of geomaterials. Support is provided by the Center for Research in Earth and Space Technology (CRESTech), Natural Sciences and Engineering Research Council of Canada (NSERC), the Canadian Foundation for Innovation (CFI), INCO Limited, Ministry of Northern Development and Mines (MNDM), Dillon/Hyd-Eng Geophysics Inc., National Research Council (NCR), and PDVSA INTEVEP S.A. Their support for this project is very much appreciated.

Notation

The following symbols are used in this paper:

A = spectral amplitude;
$[C]$ = damping matrix;
D = damping ratio;
$\overline{D}$ = average damping ratio;
d = distance from receiver;
E = Young's modulus;
e = void ratio;
F = loading force;
$\{F\}$ = forcing function;
F_b = force magnitude;
f = frequency;
$f_{\max}$ = highest propagating frequency;
G = shear modulus;
Ge = spectral amplitude of geometrical spreading, reflections, etc.;
g = largest element dimension;
$[K]$ = stiffness matrix;
$[M]$ = mass matrix;
Q = quality factor;
R = constant dependent on V_P, V_S, and V_R;
T = period;
t = time;
u = displacement;
$\dot{u}$ = velocity;
$\ddot{u}$ = acceleration;
V = velocity;
V_P = compression wave velocity;
V_R = Rayleigh wave velocity;
V_S = shear wave velocity;
x = distance;
α = Newmark-β parameter;
$\alpha_{t,x}$ = attenuation coefficient in time and distance;
β = Newmark-β parameter;
ΔD = relative damping ratio;
Δx = distance between two measurements;
η = Rayleigh damping parameters;
λ = wavelength;
$\lambda_{\min}$ = minimum wavelength;
ν = Poisson's ratio;
ρ = density;
σ = damping ratio variance;
τ = characteristic time;
χ = constant dependent on consistent or lumped mass matrices;
ψ = function of pulse width; and
ω = rotational frequency.

References

Al-Hunaidi, M. O. (1993). "Insights on the SASW nondestructive testing method." *Can. J. Civ. Eng.*, 20, 940–950.

Båth, M., and Berkhout, A. J. (1984). *Mathematical aspects of seismology*, Klaus Helbig and Sven Trietel, eds., Geophysical, London.

Cascante, G., and Santamarina, J. (1997) "Low strain measurements with a resonant-column apparatus." *Geotech. Test. J.*, 20(1), 29–39.

Cascante, G., Hutchinson, J., and Phillips, C. (1999) "Assessment of the spectral analysis of surface waves method for detecting underground voids." *Proc., 52nd Canadian Geotechnical Conf.*, Regina, Saskatchewan, Canadian Geotechnical Society, Toronto, 49–53.

Caughey, T. K. (1960). "Classical normal modes in damped linear systems." *J. Appl. Mech.*, 27, 269–271.

Gucunski, N., and Woods, R. D. (1992). "Numerical simulation of the SASW test." *Soil Dyn. Earthquake Eng.*, 11, 213–227.

Lamb, H. (1904). "On the propagation of tremors over the surface of an elastic solid." *Philos. Trans. R. Soc. London, Ser. A*, 203, 1–42.

Léger, P., and Dussault, S. (1992). ''Seismic-energy dissipation in MDOF structures.'' *J. Struct. Eng.*, 118(5), 1251–1269.
Liu, M., and Gorman, D. G. (1995). ''Formulations of Rayleigh damping and its extensions.'' *Comput. Struct.*, 57(2), 277–285.
Marfurt, K. J. (1984). ''Accuracy of finite-difference and finite element modeling of the scalar elastic wave equations.'' *Geophysics*, 49(5), 533–549.
Phillips, C., Cascante, G., and Hutchinson, J. (2000). ''Assessment of the spectral analysis of surface waves method for detecting underground voids.'' *Annual Symposium on the Application of Geophysics to Environmental and Engineering Problems*, Arlington, Va., Environmental and Engineering Geophysical Society, Denver, 29–37.
Rix, G. J., and Stokoe, II, K. E. (1989). ''Stiffness profiling of pavement subgrades.'' *Transp. Res. Rec.*, 1235, 1–9.
Saenger, E. H., Gold, N., and Shapiro, S. A. (2000). ''Modeling the propagation of elastic waves using a modified finite-difference grid.'' *Wave Motion*, 31, 77–92.
Toksöz, M. N., Johnston, D. H., and Timur, A. (1979). ''Attenuation of seismic waves in dry saturated rocks: I. Laboratory measurements.'' *Geophysics*, 44, 681–690.
Valliappan, H. S., and Murti V. (1984). ''Finite element constraints in the analysis of wave propagation problems.'' *UNICIV Rep. No. R-218*, School of Civil Engineering, Univ. of New South Wales, New South Wales, Australia.
Wang, Y. C., Murti, V., and Valliappan, S. (1992). ''Assessment of the accuracy of the Newmark method in transient analysis of wave propagation problems.'' *Earthquake Eng. Struct. Dyn.*, 21, 987–1004.
Ward, R. W., and Toksöz, M. N. (1971). ''Causes of regional variation of magnitude.'' *Bull. Seismol. Soc. Am.*, 61, 649–679.
Woodward, P. K., and Griffiths, D. V. (1996). ''Influence of viscous damping in the dynamic analysis of an earth dam using simple constitutive models.'' *Comp. Geotechn.*, 19(3), 245–263.
Zerwer, A., Polak, M. A., and Santamarina, J. C. (2000). ''Experimental investigation of wave propagation in thin Plexiglas plates: Implications for modeling and measuring Rayleigh waves.'' *NDT & E Int.*, 33, 33–41.